Optical properties of magnesium doped Al x Ga1− x N (0.61 ≤ x ≤ 0.73)

Martin Feneberg, Sarah Osterburg, María Fátima Romero, Bernd Garke, Rüdiger Goldhahn, Maciej D. Neumann , Norbert Esser, Jianchang Yan, Jianping Zeng, Junxi Wang, and Jinmin Li

Citation: Journal of Applied Physics **116**, 143103 (2014); doi: 10.1063/1.4897449
View online: http://dx.doi.org/10.1063/1.4897449
View Table of Contents: http://scitation.aip.org/content/aip/journal/jap/116/14?ver=pdfcov
Published by the AIP Publishing

Optical properties of magnesium doped $Al_xGa_{1-x}N$ ($0.61 \leq x \leq 0.73$)

Martin Feneberg,[1,a)] Sarah Osterburg,[1] María Fátima Romero,[1] Bernd Garke,[1] Rüdiger Goldhahn,[1] Maciej D. Neumann,[2] Norbert Esser,[2] Jianchang Yan,[3] Jianping Zeng,[3] Junxi Wang,[3] and Jinmin Li[3]

[1]*Institut für Experimentelle Physik, Otto-von-Guericke-Universität Magdeburg, Universitätsplatz 2, 39106 Magdeburg, Germany*

[2]*Leibniz-Institute for Analytical Sciences—ISAS—e.V., Albert-Einstein-Str. 9, 12489 Berlin, Germany*

[3]*Semiconductor Lighting R&D Center, Institute of Semiconductors, Chinese Academy of Sciences, People's Republic of China*

(Received 25 July 2014; accepted 27 September 2014; published online 9 October 2014)

We investigate the optical properties of $Al_xGa_{1-x}N$:Mg with aluminum content of $0.61 \leq x \leq 0.733$ in comparison to undoped and silicon doped reference samples. The ordinary dielectric functions, excitation, and emission spectra are reported at different temperatures. A comprehensive analysis yields quantitative data on the valence band structure of the ternary alloy, i.e., splitting and order of valence bands with different symmetries. Finally, the near band gap emission in AlGaN:Mg is found to be most probably dominated by donor to free-hole recombination. © *2014 AIP Publishing LLC*. [http://dx.doi.org/10.1063/1.4897449]

I. INTRODUCTION

Increasing interest in ultraviolet (UV) light emitting diodes has led to great efforts in the development of doped $Al_xGa_{1-x}N$ layers. While n-type doping with silicon has frequently been reported with reasonable success,[1–4] p-type doped $Al_xGa_{1-x}N$ is apparently much harder to achieve. For implementation of doped $Al_xGa_{1-x}N$ layers into functional devices like light emitting diodes or laser diodes, the optical properties of the doped injection layers have to be understood in detail. Very important are therefore the knowledge of the dielectric function, splittings and oscillator strengths of interband transition energies, and recombination mechanisms. Yet there are no data available how doping, especially by the acceptor candidate Mg, influences these important optical properties.

Here, we present a systematic study on optical properties of $Al_xGa_{1-x}N$:Mg ($x = 0.61$, 0.66, and 0.733) and compare to $Al_{0.66}Ga_{0.34}N$:Si and unintentionally doped (UID) $Al_{0.66}Ga_{0.34}N$. By a combination of spectroscopic ellipsometry and photoluminescence excitation spectroscopy (PLE), we are able to determine the valence band sub-structure of the samples which is supported by **kp** theoretical calculations. This allows to analyze localization effects in the emission properties correctly. With Mg doping, the luminescence spectra change their structure from broad unstructured bands in UID or Si doped to structured emission in Mg doped samples. The corresponding luminescence mechanism in $Al_xGa_{1-x}N$:Mg is discussed, where we propose a neutral donor to free-hole transition being responsible for the new arising bands at the low energy wing of the near band edge emission.

II. STRUCTURAL PROPERTIES AND EXPERIMENTAL

Three Mg-doped AlGaN samples with different Al composition were grown on (0001) sapphire substrates by low pressure (50 Torr) metal organic chemical vapor deposition.[5] A thin AlN buffer layer of about 80 nm thickness grown at 600 °C was used to initiate the growth. A 1 μm AlN layer grown at 1200 °C was used as high temperature template followed by a 1.2 μm thick Mg-doped AlGaN layer grown under 1000 °C. Trimethyl aluminum (TMA), trimethyl gallium, and ammonia were used as Al, Ga, and nitrogen sources. High purity H_2 served as the carrier gas. Biscyclo-pentadienyl magnesium (Cp_2Mg) was used as source for Mg doping. The magnesium concentration in the semi-insulating layers was estimated to be on the order of $5 \times 10^{19}\,cm^{-3}$ from growth parameters. The three Mg-doped $Al_xGa_{1-x}N$ samples were grown under the same conditions, except the flow rate of TMA which was varied leading to different aluminum compositions (x). A TMA flow of 12 sccm led to $x = 0.610$, 20 sccm to $x = 0.660$, and 35 sccm to $x = 0.733$, respectively. Additionally, an unintentionally doped (UID) $Al_{0.66}Ga_{0.34}N$ sample and a silicon doped $Al_{0.66}Ga_{0.34}N$ sample have been investigated for comparison.

The Al composition and the structural quality of the samples were determined by high-resolution x-ray diffraction (Bede D1 HR-XRD) using Cu K_α radiation. Rocking curves were recorded for the symmetric (002) and the skew-symmetric (102) reflections, as well as reciprocal space maps (RSM) for the asymmetric (105) reflections (not shown here). According to the (105) asymmetrical XRD RSMs obtained from the three Mg-doped AlGaN samples, the AlN template reciprocal lattice points are not in vertical alignment with that of the AlGaN epilayers, indicating that AlGaN is not pseudomorphically strained on the AlN template. The Al composition was calculated and is summarized in Table I together with lattice parameters and rocking curve full widths at half maximum (FWHM) values. The (002) and (102) rocking curves are presented in Fig. 1. For the (002) rocking curves a detector slit of 0.5 mm was used, while for the (102) rocking curves the detector was open. This fact is visible by the presence of a part of the AlN layer reflex in

[a)]Author to whom correspondence should be addressed. Electronic mail: martin.feneberg@ovgu.de

TABLE I. Summary of structural properties of the $Al_xGa_{1-x}N$:Mg layers and results from **kp** theoretical calculations. E_j ($j = \Gamma_{7+}, \Gamma_9, \Gamma_{7-}$) are the transition energies (at $T = 10$ K), $O_{j,\perp}$ the relative oscillator strengths for $\mathbf{E} \perp \mathbf{c}$ and $O_{j,\parallel}$ these for $\mathbf{E} \parallel \mathbf{c}$ for the transitions from the conduction band to the valence band indicated in the index.

Al content x	0.610	0.660	0.733
TMA flow (sccm)	12	20	35
a (Å)	3.119	3.119	3.120
c (Å)	5.083	5.066	5.049
ϵ_{xx}	-7.4×10^{-3}	-6.1×10^{-3}	-4.0×10^{-3}
ϵ_{zz}	4.4×10^{-3}	3.1×10^{-3}	2.7×10^{-3}
(002)FWHM (arc sec)	380.4	414.5	337.8
(102)FWHM (arc sec)	599.3	679.3	608.4
$E_{\Gamma_{7+}}$ (eV)	5.002	5.120	5.278
E_{Γ_9} (eV)	5.031	5.181	5.378
$E_{\Gamma_{7-}}$ (eV)	5.043	5.191	5.387
$O_{\Gamma_{7+},\perp}$	0.015	0.005	0.002
$O_{\Gamma_9,\perp}$	0.500	0.500	0.500
$O_{\Gamma_{7-},\perp}$	0.485	0.495	0.498
$O_{\Gamma_{7+},\parallel}$	0.971	0.991	0.996
$O_{\Gamma_9,\parallel}$	0.000	0.000	0.000
$O_{\Gamma_{7-},\parallel}$	0.029	0.009	0.004

the (102) data only (on the right hand side in Fig. 1). We found no definite links between FWHM and the Al content. The densities of screw threading dislocations (TDs) and edge TDs were estimated to be $6 - 9.5 \times 10^8\,cm^{-2}$ and $1.2 - 1.7 \times 10^8\,cm^{-2}$ from FWHMs of rocking curves, respectively.

All samples have been studied by temperature dependent photoluminescence (PL) spectroscopy, and spectroscopic ellipsometry. PL was excited by an ArF^* excimer laser ($\lambda = 193$ nm), while the sample was mounted inside a temperature variable liquid helium cooled cryostat. Emitted light was dispersed by a grating monochromator and detected by a liquid nitrogen cooled charge-coupled device camera. Spectroscopic ellipsometry was performed at two different

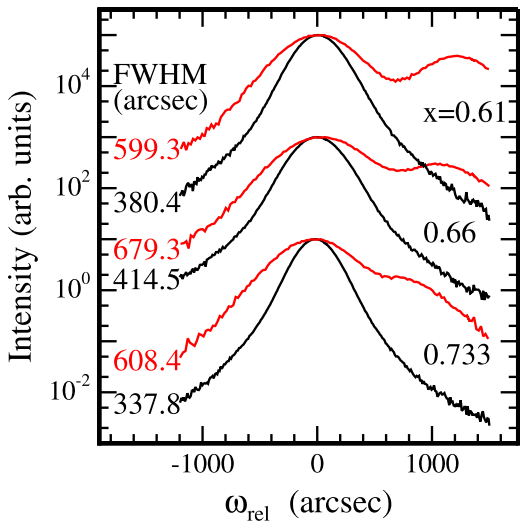

FIG. 1. XRD ω-rocking curves for (002) reflections (black curves) and (102) reflections (red curves) of the three Mg-doped AlGaN samples grown on (0001) sapphire substrate, with the corresponding FWHM value of the (002) and (102) Bragg peaks given on the left side.

setups. In the spectral range from 0.5 to 6.5 eV, we used a commercial variable angle spectroscopic ellipsometer (Woollam). Data for photon energies between 4.9 and 9.8 eV were recorded by an ellipsometer[6] mounted at the synchrotron beamline U125/2-NIM at the Berlin electron storage ring for synchrotron radiation (BESSY II, Germany). While the angle of incidence was varied for the laboratory setup, at the BESSY II ellipsometer it was fixed to 67.5°. All ellipsometric data presented here refer to room temperature ($T = 295$ K) except for Fig. 6 and the lower trace in Fig. 7. The ordinary dielectric function was extracted from the ellipsometric parameters Ψ and Δ using a multi-layer fit procedure as published earlier[7] employing model dielectric functions. Finally, PLE was recorded at the synchrotron light source DORIS III at DESY, Hamburg (Germany) using the superlumi station at beamline I at 10 K (and at 295 K for the upper trace in Fig. 7). Details can be found elsewhere.[8,9]

III. RESULTS AND DISCUSSION

In order to get a first insight into the expected emission and absorption properties in the range of the fundamental band gap, it is essential to consider the valence band ordering at the Γ points of the Brillouin zone and the polarization dependent transition probabilities into the conduction band.

We use the known alloy composition and lattice parameters (Table I) of the biaxially compressively strained films to calculate the valence band structure and thus the transition energies (Table I). Theoretical model calculations by the **kp** method are performed using an approach published earlier making use of exciton transition energies.[10] A band gap bowing of $b = 0.9$ eV (Ref. 11) is adopted describing the transition from the conduction band to the valence band having Γ_9 symmetry according to Eq. (1). Unstrained lattice parameters are interpolated linearly between values from Ref. 12 for GaN and Ref. 13 for AlN. All used parameters are summarized in Table II. For the alloy composition range investigated in this study, the valence band order is the same as for AlN. We thus have a lowest energy transition between the conduction band and valence band with Γ_7 symmetry (to distinguish the two transitions involving Γ_7 valence bands, we label them in indices as + and − by increasing energy). The relative oscillator strengths of these transitions were also

TABLE II. Parameters entering in **kp** theoretical calculations. For $Al_xGa_{1-x}N$, the parameters are linearly interpolated.

	GaN	AlN
E_{Γ_9} (room temp.)	3.412 eV (Ref. 14)	6.183 eV (Ref. 15)
E_{Γ_9} (low temp.)	3.478 eV (Ref. 14)	6.255 eV (Ref. 15)
b	0.9 eV (Ref. 11)	
Δ_{cf}	12.3 meV (Ref. 16)	−221 meV (Ref. 15)
Δ_{so}	16.7 meV (Ref. 16)	13 meV (Ref. 15)
$a - D_1$	−6.5 eV (Ref. 16)	−6.9 eV (Ref. 10)
$a - D_2$	−11.2 eV (Ref. 16)	−15.2 eV (Ref. 10)
D_3	4.9 eV (Ref. 16)	8.3 eV (Ref. 10)
D_4	−5.0 eV (Ref. 16)	−4.15 eV (Ref. 10)
a	3.18926 Å (Ref. 12)	3.11197 Å (Ref. 13)
c	5.18523 Å (Ref. 12)	4.98089 Å (Ref. 13)

calculated and found to decrease for increasing aluminum concentration for $\mathbf{E} \perp \mathbf{c}$ (Table I, $O_{\Gamma_{7+},\perp}$). The ellipsometric results presented here are therefore mainly sensitive to transitions from lower energy valence bands, the onset will be dominated by the valence band having Γ_9 symmetry as discussed in Ref. 17. The calculated energy situation at room temperature is presented in Fig. 2. There, symbols represent the values for the specific samples and the continuous lines an unstrained reference case. In PLE, we find the absorption onset dominated by the transition from the highest valence band as will be discussed below.

A. Dielectric function

The complex ordinary dielectric functions (DFs, $\bar{\varepsilon} = \varepsilon_1 + i\varepsilon_2$) of the three $Al_{0.66}Ga_{0.34}N$ layers are compared in Fig. 3. We observe no clear excitonic features at the band edge, i.e., in ε_2 there is a step-like increase around the band gap which can be interpreted as broadened excitons superimposed to the onset of the exciton continuum. Differences between the energy positions of the absorption onsets are attributed to small differences in aluminum concentrations or strain. This is in line with x-ray diffractometry results and most likely caused by different Al intake due to chemical variations of the gas phase by presence of Si or Mg dopants. More striking are the changes of the above gap absorption due to different dopants. While both UID $Al_{0.66}Ga_{0.34}N$ and $Al_{0.66}Ga_{0.34}N$:Si reach a value of $\varepsilon_2 = 1.76$ at 5.5 eV, the $Al_{0.66}Ga_{0.34}N$:Mg layer has only $\varepsilon_2 = 1.48$. Its absorption remains weaker for increasing photon energies up to around 7.8 eV where the situation changes. Redistribution of oscillator strength also is observable at these higher photon energies. At around 8.5 eV Si doping seems to decrease, while Mg doping increases the oscillator strength, while all kind of doping leads to increasing broadening of features. The reason for the observed redistribution of oscillator strength

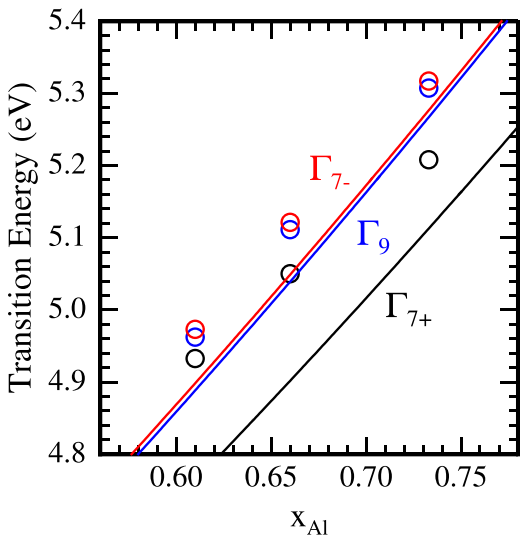

FIG. 2. Transition energies ($T = 295$ K) of the strained samples (open circles) and unstrained reference values (continuous lines) calculated by **kp** theory. The relative oscillator strength of the lowest transition (marked Γ_{7+}, black) is close to zero for $\mathbf{E} \perp \mathbf{c}$, an absorption experiment is therefore sensitive to the transition marked as Γ_9 (blue).

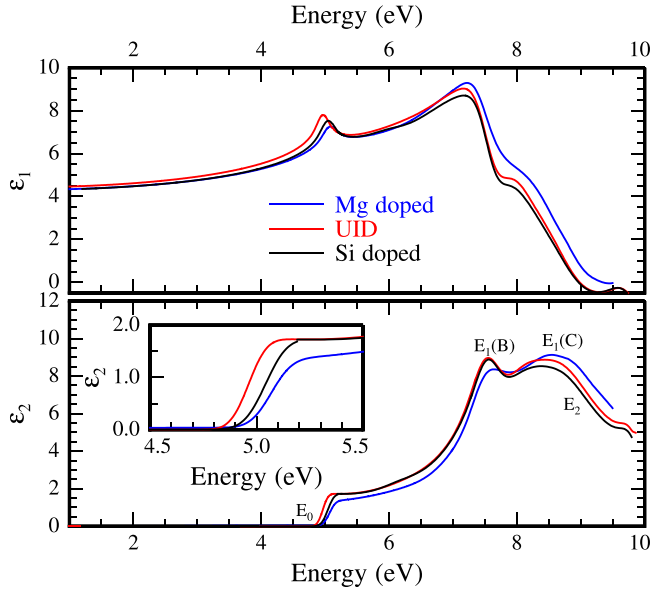

FIG. 3. Ordinary dielectric functions of the samples with $x = 0.66$. The different dopants are given in the figure.

remains unclear at the moment. The behavior of ε_1 (related to the refractive index) below the band gap is determined by the energy position and amplitude of the high energy feature $E_1(B)$ at around 7.5 eV rather than by the amplitude of ε_2 above the gap.

In a next step, we compare the ordinary DFs of $Al_xGa_{1-x}N$:Mg layers with $x = 0.61$, 0.66, and 0.733 with those of GaN and AlN.[15] Please note that $x = 0.66$ refers to the same sample as in Fig. 3. In Fig. 4 the DFs are upshifted (not to scale) to make the energy positions of their features better visible. High energy features are again shifted due to the concentration of the layers, visible both in ε_1 and ε_2. The exact energy values for the features in the DFs were obtained by a method described in detail earlier.[11] In the same

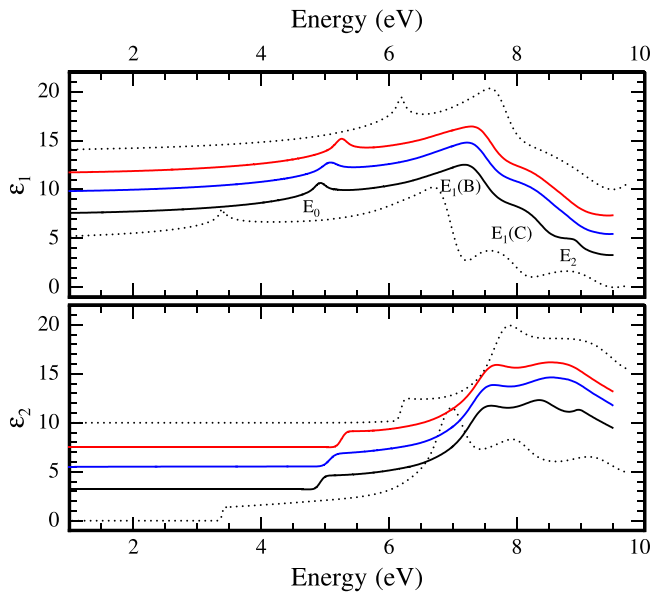

FIG. 4. Ordinary dielectric functions of the AlGaN:Mg samples with $x = 0.61$ (black), 0.66 (blue), and 0.733 (red) in comparison to GaN and AlN (both dotted). The curves are vertically shifted to enhance visibility.

reference already critical points for $Al_xGa_{1-x}N$ ($0.11 \leq x \leq 0.53$) have been analyzed which we adopt here. The resulting energies as a function of alloy composition are presented in Fig. 5. The nonlinear interpolation of the high energy features is expressed by the usual bowing relation also valid for the band gap

$$E(Al_xGa_{1-x}N) = xE(AlN) + (1-x)E(GaN) - bx(1-x), \quad (1)$$

where b denotes the bowing parameter and E represents the energy of the discussed feature. For the different transitions these bowing parameters are $b = 0.9$ eV (E_0, fundamental band gap), 0.2 eV ($E_1(B)$), 0.1 eV ($E_1(C)$), and 0.5 eV (E_2). The labeling is done according to Ref. 15. Corresponding interpolation curves are also shown in Fig. 5. Note, that already in zincblende $Al_xGa_{1-x}N$ alloys the behavior that E_2 was shifting to smaller energies with increasing aluminum content, while all other contributions show an upward shift confirmed by both experiments and theory.[18]

B. Valence band splitting

Next, we contribute experimentally to the ongoing discussion of the valence band sub-structure in AlGaN. The calculated results in Fig. 2 (at room temperature) show an order of the valence bands as in AlN.[9] Ellipsometry results show unambiguously the absorption onset related with the Γ_9 valence band.[19] This transition is shown as a function of temperature in Fig. 6 for the Mg doped sample with $x = 0.733$. The overall shift of the characteristic energy amounts to 75 meV from low to room temperature and follows the Viña relation.[20] This is very similar to the value for AlN which is reported to be 74 meV.[21]

Additional data obtained by PLE at low temperature are compared in the next step. The direct comparison of spectra obtained by both techniques is presented in Fig. 7. The PLE detection window was shifted from the low temperature value of 3.59 eV to 3.44 eV at room temperature. In Fig. 7, it can be clearly seen that the PLE onset occurs at lower energy than the absorption onset characterized by the dielectric function. This behavior can be explained by comparison with calculated transition energy values (marked by arrows in Fig. 7). The PLE onset obviously is related to the transition with participation of the Γ_{7+}valence band.

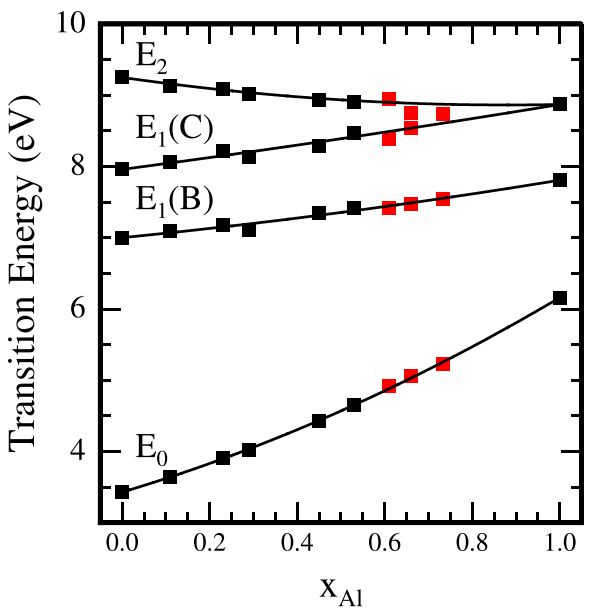

FIG. 5. High energy features of the ordinary dielectric function as a function of alloy composition for $Al_xGa_{1-x}N$. Black symbols refer to the results from Ref. 11, red symbols to the data points of this work.

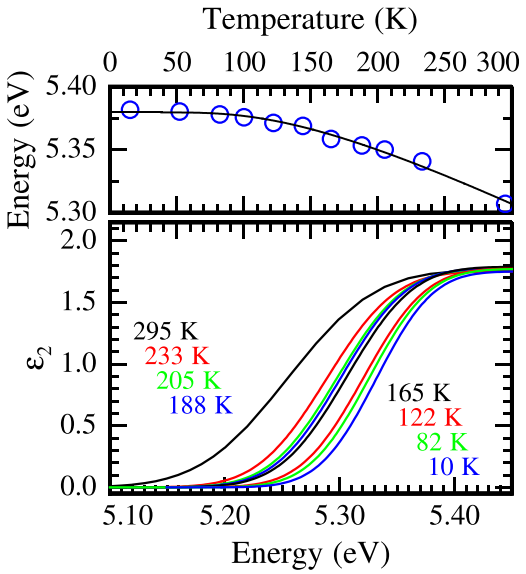

FIG. 6. Imaginary part of the dielectric functions obtained at different temperatures for $Al_{0.733}Ga_{0.267}N$:Mg. The ε_2 traces for $T = 295$ K and 10 K are compared to excitation spectra in Fig. 7. The temperature dependence of the absorption onset is reported in the upper tableau. An overall change of ≈75 meV is found.

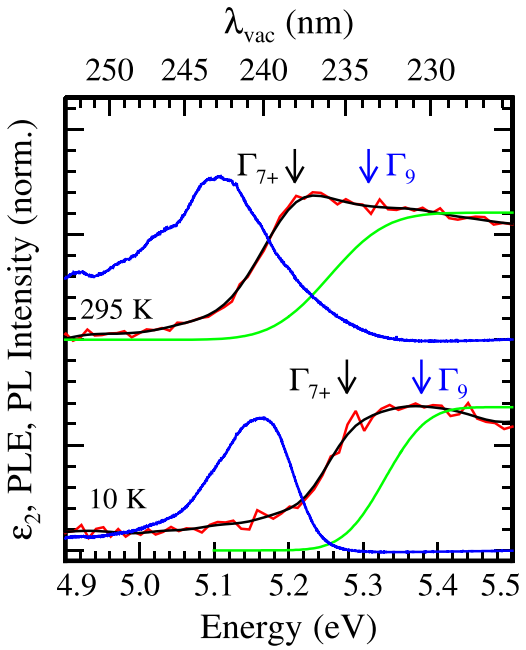

FIG. 7. Direct comparison of photoluminescence excitation spectra (black and red curves) and the imaginary part of the dielectric functions (green curves) at low and room temperature for $Al_{0.733}Ga_{0.267}N$:Mg. PLE monitors are at 3.59 eV (low temperature) and 3.44 eV (room temperature). Photoluminescence is also shown for comparison (in blue). The arrows mark the calculated transition energies between conduction band and the first two valence sub-bands.

The experimental configuration used for recording PLE is sensitive to a superposition of light absorption polarized along $\mathbf{E} \perp \mathbf{c}$ and $\mathbf{E} \parallel \mathbf{c}$.[9] The relative oscillator strengths given in Table I for the transition from the highest valence band into the conduction band ($O_{\Gamma 7+,\perp}$) are therefore lower limits. In Fig. 8, we demonstrate PLE spectra of all three $Al_xGa_{1-x}N$:Mg samples and mark the calculated transitions by arrows.

An estimate of the relative absorption strength based on adding oscillator strengths according to Malus' law for an angle of incidence of 35° on the sample surface[9]—corresponding approximately to 15° inside the sample—yields for about 50% increased values for the lowest energy transition and a reduced value for the transition related to the valence band with Γ_9 symmetry compared to the oscillator strength for $\mathbf{E} \perp \mathbf{c}$. An additional but unknown factor increasing the PLE sensitivity to the highest valence band is the luminescence mechanism of the channel observed to record PLE spectra. The detection windows for PLE were centered at 3.59 eV ($x = 0.733$), 4.07 eV ($x = 0.66$), and 3.49 eV ($x = 0.61$), respectively, representing low energy defect recombination bands to allow for measuring the full band gap spectral region. If the monitored low energy defect band is strongly associated with the highest valence band, a further increase in PLE sensitivity to this transition would be natural.

The corresponding PL spectra are also shown in Figs. 7 and 8. A significant Stokes shift is found, i.e., an energy separation between the characteristic energy of the PLE edge and the peak position of PL. At low temperature (Fig. 8), the energy distances of 146, 164, and 118 meV are found for increasing aluminum concentration. Additionally, for $Al_{0.733}Ga_{0.267}N$:Mg we measure a value of 103 meV at room temperature (Fig. 7). The photoluminescence signal can therefore not be related to band-to-band or free exciton recombination, but additional localization effects have to be considered.

C. Temperature dependence of emission

Photoluminescence spectra were recorded at variable temperatures from $T = 5$ K up to room temperature for all samples. In Fig. 9, a comparison of the near band-gap signals from the differently doped samples at same aluminum concentration ($x = 0.66$) is shown. We observe a continuous energy shift to lower energies with increasing temperature due to increasing electron-phonon interaction. The UID and the silicon doped samples exhibit very similar behavior. Both show a broad unstructured PL band, whose peak energies decrease for about 30–40 meV for the full temperature range. This is lower than the decrease of the band gap due to electron-phonon interaction which amounts to 75 meV for the ordinary absorption edge in the samples with $x = 0.733$ (see above). In contrast, the Mg doped sample exhibits a PL band containing several distinguishable sub-structures. At above ≈ 100 K a lower energy contribution dominates the spectrum. The overall peak shift amounts to 72 meV, while the high energy wing undergoes a shift similar to the spectra from UID and Si doped samples. We assign the small absolute temperature dependent shift to localization in the ternary alloy material[22] which is as well a probable cause for a part of the observed large Stokes shifts.

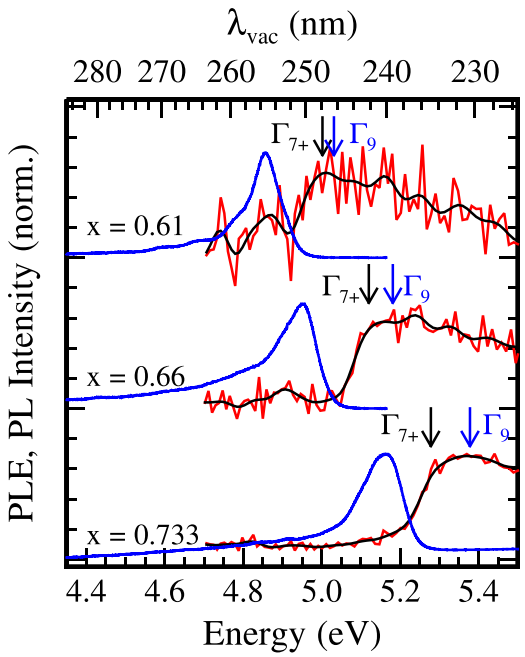

FIG. 8. Low temperature ($T = 10$ K) comparison of photoluminescence (blue curves) and photoluminescence excitation (PLE, red curves) spectra of $Al_xGa_{1-x}N$:Mg. All spectra are normalized and shifted vertically. The original PLE spectra are superposed by averaged curves (black) to enhance visibility. The arrows mark the calculated low temperature interband transition energies related to the highest valence band (with Γ_{7+} symmetry, black arrow) and the second valence band (with Γ_9 symmetry, blue arrow). PLE monitors are at 3.49 eV, 4.07 eV, and 3.59 eV for increasing x.

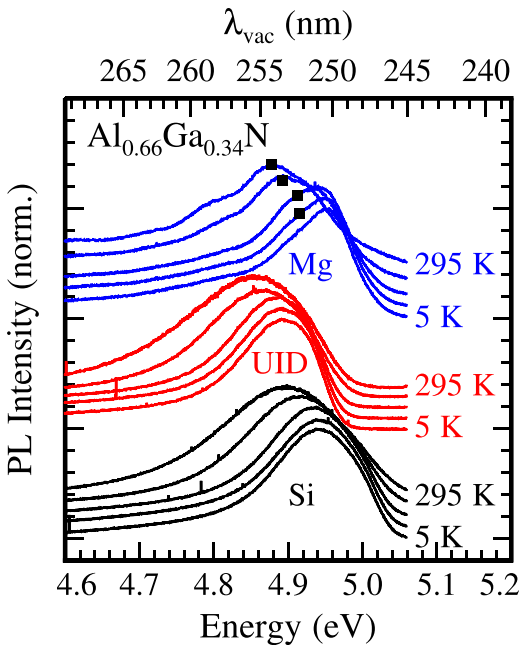

FIG. 9. Normalized photoluminescence spectra of $Al_{0.66}Ga_{0.34}N$ at different selected temperatures (from bottom to top: 5 K, 50 K, 100 K, 200 K, and 295 K, respectively). The spectra are normalized and shifted vertically for better visibility. For the Mg doped sample (top, blue) the maxima of the low energy contribution dominating at elevated temperatures are marked by symbols as a guide to the eye.

The obvious influence of Mg doping on the PL spectra is the occurrence of the distinguishable low energy side band. This finding is in agreement with earlier published work by Suzuki *et al.*[23] who presented comparable spectra of $Al_{0.94}Ga_{0.06}N$:Mg, namely the occurrence of an additional peak after Mg doping at lower energy than the main near band-gap contribution. The origin of this peak was however not unambiguously clarified yet. Suzuki *et al.*[23] discussed the possibility of a free-electron to neutral acceptor ($e^- A^0$) transition as origin of the band. The acceptor ionization energy E_A can then be estimated by the distance ΔE of the low energy shoulder to the main near band gap recombination because both bands would be subject to the same localization effects.

To test this hypothesis, we extract the energy differences between main near band gap emission peak and the Mg related shoulder in all our $Al_xGa_{1-x}N$:Mg samples. Temperature dependent spectra are shown in Fig. 10. The spectra were fitted by several Gaussian bands to account for the different contributions including phonon replicas. The distances between these bands are within fitting accuracy (± 10 meV) constant as a function of temperature and are $\Delta E = 50$ meV for $x = 0.61$, 45 meV for $x = 0.66$, and 85 meV for $x = 0.73$. However, the fits for sample A ($x = 0.61$) are less reliable as peak assignment is difficult in the PL spectra because no clear change in the dominant peak is found for this sample. Here, we suspect already at low temperature the Mg-related peak to be dominant and measure the distance ΔE instead to the weak high energy shoulder. Nevertheless, the relative low values of ΔE are in conflict to expected Mg acceptor activation energies of >250 meV. Earlier reports relying on cathodoluminescence spectra yielded values of $E_A \approx 700$ meV for our alloy concentration range.[24]

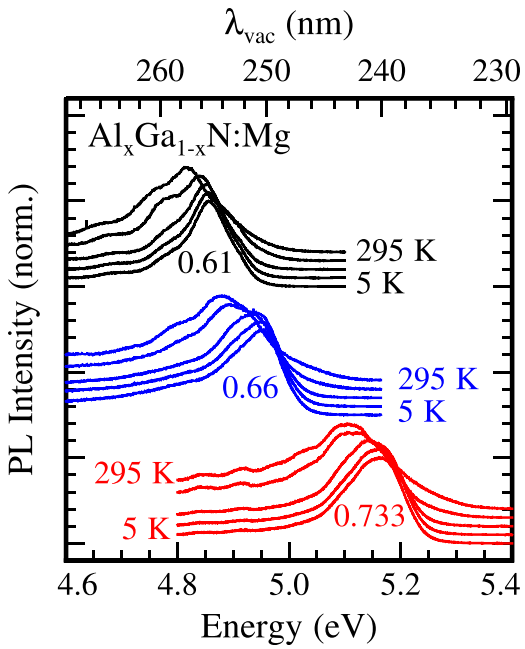

FIG. 10. Normalized photoluminescence spectra of $Al_xGa_{1-x}N$:Mg at different selected temperatures (from bottom to top: 5 K, 50 K, 100 K, 200 K, and 295 K, respectively). The spectra are shifted vertically for better visibility. In the spectra for $x = 0.733$ and 0.66 the transition to the dominating low energy transition at elevated temperatures is clearly visible. For $x = 0.61$ the same transition dominates at low and at room temperature.

Alternatively, Mg related bound exciton emission was mentioned by Suzuki *et al.*[23] as a possible origin. In favour of this interpretation are the small values of ΔE which then resemble exciton localization energies which are according to Haynes' rule[25] dependent on the acceptor ionization energy. The latter cannot be directly determined from ΔE alone. However, it remains unclear why the acceptor bound exciton would increase in relative intensity with increasing temperature. For acceptor bound exciton emissions we expect the opposite behavior.

We therefore put forward a third interpretation. Incorporation of Mg acceptor centers in AlGaN lowers the Fermi energy. Thus facilitated incorporation of compensating donors like Si_{Al} and O_N is probable, similar to the case of AlN.[26] We propose the acceptor centers introduced by Mg doping are optically inactive around the band edge, i.e., they mainly contribute to nonradiative centers[23] or cluster.[27] The additionally introduced *donors* would therefore probably dominate the emission properties of such AlGaN layers. We are well aware of the ongoing discussion if Si_{Al} and O_N are incorporated as shallow donors or deep DX centers in AlN and high Al content AlGaN,[28,29] however a neutral donor to free-hole transition (h^+D^0) would be possible in both cases supported by an increased hole concentration due to Mg doping. The energy distance from the additional luminescence band to the main near band gap recombination would then resemble the *donor* ionization energy E_D instead of E_A. Our estimated values between 45 and 85 meV are in reasonable agreement to earlier published donor activation energies in AlGaN of similar composition both for Si_{Al} (Ref. 30) and for O_N.[31] The temperature dependence of the PL spectra (Fig. 10) also supports the interpretation of the low energy wing recombination bands as h^+D^0 transitions. From Arrhenius analysis of the peak intensities we estimated the activation energies of the h^+D^0 transitions. It is found that the activation energies are identical to ΔE values as given above. This means the donor activation is the most important quenching process of the h^+D^0 recombination channel while the decreasing intensity of the main near band gap emission can at the same time be explained by a possible large lattice relaxation of shallow donors to DX centers and/or by increasing nonradiative recombination via deep centers introduced by Mg doping.

IV. SUMMARY

We have studied the optical properties of $Al_xGa_{1-x}N$:Mg thin films with aluminum content of $0.61 \leq x \leq 0.733$ in comparison to unintentionally and silicon doped $Al_{0.66}Ga_{0.34}N$ layers. We have discussed differences in the dielectric functions of $Al_{0.66}Ga_{0.34}N$ due to different dopant incorporation which occur partly as additional broadening mechanism above the band gap. Additionally, the aluminum concentration dependence of high energy features in the dielectric function was determined where we complemented earlier published results.[11] The valence band ordering of the Mg-doped samples was determined by means of

spectroscopic ellipsometry and photoluminescence excitation spectroscopy. We have shown that the ordinary dielectric function is sensitive to the transition involving the valence band with Γ_9 symmetry, while PLE sets already in for the higher valence band with Γ_7 symmetry. Photoluminescence spectra of all samples were presented at different temperatures. We identified a low energy wing of the near band-edge emission as being caused by Mg doping and discussed its origin. The most likely identification of the band is a neutral donor to free-hole transition mirroring the donor activation energy rather than the Mg-acceptor activation energy. Estimated donor activation energies are in good agreement to earlier found values for similar aluminum concentrations.

ACKNOWLEDGMENTS

We gratefully acknowledge support by the Deutsche Forschungsgemeinschaft DFG in the framework of Major Research Instrumentation Program No. INST272/205-1. Part of this work was supported by the EU within the 7th RTD Framework (project RAINBOW: Contract No. PITN-GA-2008-213238). Furthermore, we gratefully acknowledge support by the synchrotron radiation sources BESSY II of Helmholtz-Zentrum Berlin (HZB) and DORIS III at DESY, Hamburg (both in Germany). DESY is a member of the Helmholtz Association (HGF). We would like to thank A. Kotlov for expert assistance in using beamline I at DESY and Benjamin Neuschl, Ingo Tischer, and Manfred Madel (all University of Ulm, Germany) for assistance during beamtime. Part of this work was supported by the National Natural Science Foundation of China (Grant No. 61376047), the National High Technology Research and Development Program of China (Nos. 2014AA032608 and 2011AA03A111).

[1]T. Taniyasu, M. Kasu, and N. Kobayashi, Appl. Phys. Lett. **81**, 1255 (2002).
[2]M. L. Nakarmi, K. H. Kim, K. Zhu, J. Y. Lin, and H. X. Jiang, Appl. Phys. Lett. **85**, 3769 (2004).
[3]R. Collazo, S. Mita, J. Xie, A. Rice, J. Tweedie, R. Dalmau, and Z. Sitar, Phys. Status Solidi C **8**, 2031 (2011).
[4]F. Mehnke, T. Wernicke, H. Pingel, C. Kuhn, C. Reich, V. Kueller, A. Knauer, M. Lapeyrade, M. Weyers, and M. Kneissl, Appl. Phys. Lett. **103**, 212109 (2013).
[5]J. Zeng, W. Li, J. Yan, J. Wang, P. Cong, J. Li, W. Wang, P. Jin, and Z. Wang, Phys. Status Solidi (RRL) **7**, 297 (2013).
[6]C. Cobet, R. Goldhahn, W. Richter, and N. Esser, Phys. Status Solidi B **246**, 1440 (2009).
[7]R. Goldhahn, Acta Phys. Pol. A **104**, 123 (2003).
[8]G. Zimmerer, Radiat. Meas. **42**, 859 (2007).
[9]M. Feneberg, M. Röppischer, N. Esser, C. Cobet, B. Neuschl, T. Meisch, K. Thonke, and R. Goldhahn, Appl. Phys. Lett. **99**, 021903 (2011).
[10]G. Rossbach, M. Feneberg, M. Röppischer, C. Werner, C. Cobet, N. Esser, T. Meisch, K. Thonke, A. Dadgar, J. Bläsing, A. Krost, and R. Goldhahn, Phys. Rev. B **83**, 195202 (2011).
[11]C. Buchheim, R. Goldhahn, M. Rakel, C. Cobet, N. Esser, U. Rossow, D. Fuhrmann, and A. Hangleiter, Phys. Status Solidi B **242**, 2610 (2005).
[12]V. Darakchieva, B. Monemar, and A. Usui, Appl. Phys. Lett. **91**, 031911 (2007).
[13]W. Paszkowicz, S. Podsiado, and R. Minikayev, J. Alloys Compds. **382**, 100 (2004).
[14]B. Monemar, P. P. Paskov, J. P. Bergman, A. A. Toropov, T. V. Shubina, T. Malinauskas, and A. Usui, Phys. Status Solidi B **245**, 1723 (2008).
[15]M. Feneberg, M. F. Romero, M. Röppischer, C. Cobet, N. Esser, B. Neuschl, K. Thonke, M. Bickermann, and R. Goldhahn, Phys. Rev. B **87**, 235209 (2013).
[16]R. Ishii, A. Kaneta, M. Funato, Y. Kawakami, and A. A. Yamaguchi, Phys. Rev. B **81**, 155202 (2010).
[17]G. Rossbach, M. Röppischer, P. Schley, G. Gobsch, C. Werner, C. Cobet, N. Esser, A. Dadgar, M. Wieneke, A. Krost, and R. Goldhahn, Phys. Status Solidi B **247**, 1679 (2010).
[18]M. Landmann, E. Rauls, W. G. Schmidt, M. Röppischer, C. Cobet, N. Esser, T. Schupp, D. J. As, M. Feneberg, and R. Goldhahn, Phys. Rev. B **87**, 195210 (2013).
[19]S. Shokhovets, R. Goldhahn, G. Gobsch, S. Piekh, R. Lantier, A. Rizzi, V. Lebedev, and W. Richter, J. Appl. Phys. **94**, 307 (2003).
[20]L. Viña, S. Logothetidis, and M. Cardona, Phys. Rev. B **30**, 1979 (1984).
[21]M. Feneberg, R. A. R. Leute, B. Neuschl, K. Thonke, and M. Bickermann, Phys. Rev. B **82**, 075208 (2010).
[22]K. B. Lee, P. J. Parbrook, T. Wang, F. Ranalli, T. Martin, R. S. Balmer, and D. J. Wallis, J. Appl. Phys. **101**, 053513 (2007).
[23]M. Suzuki, S. Sawai, K. Fukui, K. Nagamatsu, and H. Amano, Phys. Status Solidi C **6**, S759 (2009).
[24]M. Imura, N. Kato, N. Okada, K. Balakrishnan, M. Iwaya, S. Kamiyama, H. Amano, I. Akasaki, T. Noro, T. Takagi, and A. Bandoh, Phys. Status Solidi C **4**, 2502 (2007).
[25]J. R. Haynes, Phys. Rev. Lett. **4**, 361 (1960).
[26]L. Silvestri, K. Dunn, S. Prawer, and F. Ladouceur, Europhys. Lett. **98**, 36003 (2012).
[27]S. E. Bennett, P. H. Clifton, R. M. Ulfig, M. J. Kappers, J. S. Barnard, C. J. Humphreys, and R. A. Oliver, J. Phys.: Conf. Ser. **209**, 012014 (2010).
[28]C. Skierbiszewski, T. Suski, M. Leszczynski, M. Shin, M. Skowronski, M. D. Bremser, and R. F. Davis, Appl. Phys. Lett. **74**, 3833 (1999).
[29]L. Gordon, J. L. Lyons, A. Janotti, and C. G. Van de Walle, Phys. Rev. B **89**, 085204 (2014).
[30]B. Borisov, V. Kuryatkov, Yu. Kudryavtsev, R. Asomoza, S. Nikishin, D. Y. Song, M. Holtz, and H. Temkin, Appl. Phys. Lett. **87**, 132106 (2005).
[31]S. T. Bradley, S. H. Goss, L. J. Brillson, J. Hwang, and W. J. Schaff, J. Vac. Sci. Technol. B **21**, 2558 (2003).